 doi:10.20944/preprints202209.0106.v1

Tightly Coupled Ultra-Wideband Phased-Array Implemented by Three-Dimensional Inkjet Printing Technique

Lei Han[1,2], Gang Wang[1], Lin Zhang[1], Weixu Jiang[2], Pengbing Zhao[3], Wei Tang[2], Tao Dang[2], Hongxing Zheng[4]*

1. Department of Air-Defense and Anti-Missile, Air Force Engineering University, Xi'an 710100, China

2. Sichuan Jiuzhou Electric Group Co. Ltd, Mianyang 621000, China

3. School of Electro-Mechanica Engineering, Xidian University, Xi'an 710071, China

4. School of Electronics and Information Engineering, Hebei University of Technology, Tianjin 300401, China

*Correspondence: hxzheng@hebut.edu.cn; Tel.: +86-22-6043-8244

Abstract: In order to enhance the gain of antenna suitable for the airplane mounted platform, a conformal tightly coupled antenna array is investigated in this paper. Especially, three-dimensional (3-D) inkjet printing technique is used to implement the conformal property. The printing of antenna substrate and radiation layer is implemented by combining the fused deposition modelling and microdroplet injection molding technologies based on the existing 3-D printer. Here, through a unique combination of 3-D and 2-D inkjet printing of dielectric material and metallic ink, respectively, we demonstrate a monolithically integrated to a nonplanar antenna for the first time. Antenna measurements show that the complete characterization of this new process in terms of minimum feature sizes and achievable conductivities. This antenna configuration offers a high-gain performance with low-cost and rapid fabrication technique by using 3-D printing. The voltage standing wave ratio and radiation patterns are tested after adding the newly designed feed structure. Results shown the design process much efficient. Both antenna element and the array with good properties, which are in very good agreement with the specially mounted platform.

 doi:10.20944/preprints202209.0106.v1

Key words: Ultra-wideband; conformal antenna array; coupled tightly; three-dimensional printing technique; fused deposition modelling; microdroplet injection molding

1. Introduction

Tightly coupled antenna is one of the most important techniques due to its many attractive features such as high gain, wide bandwidth, and the ability to radiate both omnidirectional and directive patterns [1]. Especially, It is with more compact in size, which attracts more and more researchers who pay much attention to. Ben Munk proposed an ultra-wideband (UWB) phased array antenna based on the strong coupling effect between elements [2]. This is the proposed for the first time and design method that is fundamentally different from the traditional phased array technology, whose core idea is to intentionally increase the mutual coupling between elements in the array [3], and successfully developed an ultra-wideband 2GHz-18GHz phased array antenna prototype using this mechanism. Due to the unique advantages, more studies of tightly coupled ultra-wideband phased arrays based on this mechanism were subsequently conducted [4], [5].

With the development of wireless equipment miniaturization, the packaging of circuits and sensors embedded in conformal array antennas and electronic components was also required [6]. The gain of the antenna array can be increased by added the number of elements. However, the gain is not linearly proportional to the number of elements, and after many elements added, the size of the array is increased much more and limited it used in the space. Recently, an UWB tightly coupled phased array covering 1.2G-6GHz has been proposed, which is conformed on a cylindrical carrier and can scan up to 60°along the circumferential direction [7]. Although this antenna has achieved in bandwidth and large angle scanning,

Preprints (www.preprints.org) | NOT PEER-REVIEWED | Posted: 7 September 2022 doi:10.20944/preprints202209.0106.v1

only arranged the antenna according to the cylindrical shape, its array is relatively regular and has not made any breakthrough in the conformal of the antenna, and it is still a static-planar dipole antenna. Based on Marchand Balun and double-layered frequency selection surface (FSS) structure, a tightly coupled antenna array with ±60° angle scanning was archived in the bandwidth of 2-18GHz [8], and its profile height was 0.1λ at the lowest operating frequency only. After that, some tight-coupled arrays with lower profile that are more suitable for conformal were reported successively [9], [10]. However, these antennas have been designed independent without considering the mounted platform. In order to obtain the better performance, the conformal antenna array processed is getting more and more precise with development of the mechanism fabrication. The array must be considered with the mounted platform in the same time while designing. This is challenge problem of the antenna design. It is more difficult for us to fabricate it to fit the special mounted requirement.

In order to meet for the mounted platform, a three-dimensional (3-D) printing technology in the antennas design and fabrication came into use. The idea of mechanism fabrication of the 3-D printing technology originated with a topographic map of a layered structure, and was promoted and developed latter [11]. With the computer-aided design and manufacturing technology, the development direction of equipment printed by 3-D printing technology having been gradually from a single homogeneous material to heterogeneous multi-materials, from single to multi-processes, and from flat plane to curved surface manufactories. Traditional 3-D printing technology is a complex model sliced and then reduced to a flat graphic layup. While printing an object on the surface of the other object or

 doi:10.20944/preprints202209.0106.v1

in space to complete the total work [12], namely, conformal printing techniques have been implemented in the mechanism fabrication. However, to implement a smart control device, a conformal printing electronic circuit on mechanic structure surface is required, such as a circuit embedded in the sensor to implement the mechanic-electronic co-fabrication. Recently, Paulsen J. et al, combined 3-D printing and aerosol spray technologies to fabricate embedded circuits and sensors [13]. Kim used lead-based alloys with low melting points and additive manufacturing techniques to study the fabrication of printed circuits board (PCB) [14]. Muth et al, studied embedded 3-D printing to prepare stretchable and at the same time conformal circuits and sensors with better performance [15]. These techniques are met better for the circuits' fabrication. In some cases, the conformal antenna is always required to meet the surface of object. However, conformal printing has been less reported for antennas.

The 3-D Printing technology uses an additive process, which reduces material wastage, and by using a digitally controlled process, deposits a precise amount of material at a desired location. However, structures usually require integrated metal and dielectric, and current inkjet printing technology is still immature in depositing dielectric and metal at the same time. Inkjet printing of only dielectric materials has been used to fabricate the structures [16], [17]. On the other hand, inkjet printing of only metals has been shown to fabricate antennas on conventional planar substrates [18], [19]. There are not many reports that show the integration of inkjet-printed metal and dielectric to realize a structure. Other deposition methods such as spraying and painting have been used for the metallization of 3-D printed dielectrics [20], [21]. These methods are manual with less control over material deposition and layer thickness, and hence they cause significant material wastage. They are also not

 doi:10.20944/preprints202209.0106.v1

suitable for large-volume manufacturing. Here, a unique combination of inkjet printing of dielectric and metal has been utilized for the realization of a novel 3-D antenna configuration.

In this approach, a conformal antenna based on the tightly coupled principle is designed. The feasibility of 3-D technology combined with tightly coupled ultra-wideband antenna is investigated in detail; and the substrate and radiator of antenna are fabricated by using 3-D printing technique. For the first time, a tightly coupled antenna has been monolithically integrated to a dielectric mounted platform through inkjet printing technology. As a result of the conformal integration, a tightly coupled antenna array provides a peak gain of 12.9 dBi in the *X*-band. The characterization of the inkjet-printed 3-D dielectric material as well as inkjet-printed metal on this dielectric in terms of minimum feature sizes and conductivities has also been reported. This work shows the advantage of conformal inkjet printing technology, which has been typically limited to planar antenna designs procedures, can easily be integrated into a structure of convex shape Fabricated sample has been measured. Results are in very good agreement with simulation.

The rest of contents is organized as follows. Relationship between the elements of the tightly coupled array is analyzed in Section 2. A butterfly-shaped symmetric radiation unit is designed as a basic structure of the physed array. By using high frequency simulation system (HFSS) software, the modeling antenna is analyzed and then optimized. After simulating, the performance index of antenna element is obtained in Section 3. To obtain the conformal prototype of the tightly coupled antenna array, the property of the 3-D printer is analyzed in Section 4, the key technique of the printing has been descripted in detail. Appropriate parameters of the 3-D printer can be found in this section. To obtain excellent

Preprints (www.preprints.org) | NOT PEER-REVIEWED | Posted: 7 September 2022 doi:10.20944/preprints202209.0106.v1

performance of the array, the feed structure has been designed and discussed in 5th section. Finally, experiment results have been obtained which have been discussed in Section 6, then we conclude this approach in last section.

2. Antenna Element Structure Design

A radiation part is the basic element of the antenna array, and it is also a key component of the coupling relationship between the array elements of the tightly coupled array. Therefore, design of a tightly coupled radiation element becomes the most important research work of the tightly coupled array. To design a broadband antenna element, the most common methods is to choose the radiation body form and size with a broadband property. Traveling wave antenna and non-frequency variative antenna are the two main issues. The former is based on the current distribution without reflection, and with a very wide input impedance characteristic; and the latter essentially means that the antenna structure does not change with the electrical length. The input impedance and directional characteristic of them are broadband. Design of tightly coupled radiation element is completely different from the conventional one, which introduces strong coupling effect between each element of the array. This is mainly because increase of the impedance bandwidth of the array has to introduce an additional capacitance to offset the inductive effect raised by the reflective ground. The short dipole with overlapping structure at the end of adjacent elements is used as the array element, which can effectively widen the antenna working frequency band. On one hand, the short dipole elements are connected at the beginning and end, and the element spacing is much smaller, which can strengthen the coupling effect between elements. The overlapping

Preprints (www.preprints.org) | NOT PEER-REVIEWED | Posted: 7 September 2022 doi:10.20944/preprints202209.0106.v1

structure at the end forms a coupling capacitance, which can be used to offset the inductive effect of the reflective ground.

For the tightly coupled antenna, basic principle is shown in Figure 1. The h in the figure indicates the distance between the tightly coupled antenna element and the metal ground, the Z_{TCDA} indicates input impedance of the tightly coupled antenna element in the infinite array with the metal ground, R_{A0} and X_A indicate the radiation resistance and radiation reactance of the tightly coupled antenna element in the infinite array without the metal ground, respectively, and Z+ does the impedance when looking from the antenna plane to the metal ground. Therefore, in this array, the radiation impedance of the tightly coupled antenna element in the absence of the metal ground can be expressed as:

$$Z_{A0} = R_{A0} + jX_A \tag{1}$$

Z_{1+} can be considered as the equivalent transmission line impedance of a shorted section of termination, we have

$$Z_{1+} = j2R_{A0}\tan(\beta h) \tag{2}$$

where β is the propagation constant in free space. When the antenna is added to the metal ground, the total input impedance of the tightly coupled antenna is expressed by

$$Z_{TCDA} = jX_A + 2R_{A0}\left(j2R_{A0}\tan(\beta h)\right)/\left(2R_{A0} + j2R_{A0}\tan(\beta h)\right) \tag{3}$$

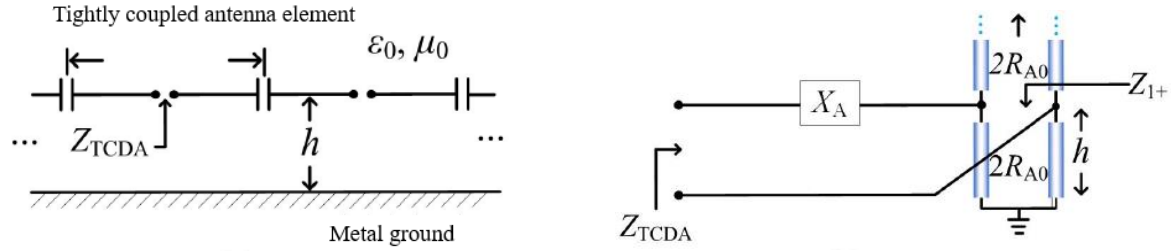

(**a**) (**b**)

Figure 1. Equivalent circuit of a tightly coupled antenna element. (**a**) infinitely large tightly coupled antenna array, (**b**) equivalent circuit diagram of the tightly coupled antenna element in the infinitely large array.

Preprints (www.preprints.org) | NOT PEER-REVIEWED | Posted: 7 September 2022 doi:10.20944/preprints202209.0106.v1

Since $2R_{A0}$ and Z_{1+} at the antenna plane are in parallel, $2R_{A0} \,||\, Z_{1+}$ presents inductance at low frequencies and capacitance at high frequencies. Since the end of the dipole antenna is loaded with capacitance, jX_A presents pure capacitance at low frequencies and pure inductance at high frequencies. When jX_A is connected in series with $2R_{A0} \,||\, Z_{1+}$, X_A can be cancelled the imaginary part of $2R_{A0} \,||\, Z_{1+}$. Therefore, tightly coupled dipole arrays can usually achieve a bandwidth of more than 4 times the frequency band, as shown in Figure 2.

According to the principle above, we design a conformal antenna which can be implemented by using the complex printing media based on 3-D printing technique. The printing media includes support medium, radiation function layer, etc. in its structure. The antenna radiating elements are printed on the surface of the support material. A space of about one-half wavelength uses a conventional array layout to form a conformal structure. A bow-tie shaped dipole is used as the basic element, as shown in Figure 3, including two pairs of vertically polarised and horizontally polarised dipole elements, the widest element size is W1, the narrow side size is W4, the total dipole size is W2, the inter-element spacing is D1 and the feed point spacing is W2.

Since the antenna array is a periodic structure, the element shape is first designed to ensure that a 2D plane is filled by translational replication. In general, the outer frame of the tightly coupled array is taken as a regular shape, and specific cells are designed within the regular frame. After the outer frame is selected, the element and spacing are determined. The size determines the minimum operating frequency of the array, the spacing is generally related to the array gate flap, and the selection of the appropriate cell spacing is related to the mutual coupling, which affects the key performance of the tightly coupled array. Then we

Preprints (www.preprints.org) | NOT PEER-REVIEWED | Posted: 7 September 2022 doi:10.20944/preprints202209.0106.v1

determine the shape of the element, because the tightly coupled antenna array is a non-resonant structure, the shape can be both bow-tie shaped broadband. At present, four kinds of basic elements are commonly used, mainly connected vibration type, oscillator type, slot slit type and bow-tie shape.

From analysis above, it can be found that the bow-tie shaped symmetric radiation element can meet the technical requirements such as the conformal shape of this project. The final structure of designed antenna element is shown in Figure 3. We have to verify this designing.

3. Simulation and Size Optimization of Antenna Element

To check the performance of the designed antenna array element above, this section mainly uses full-wave simulation software to model and optimize the simulation of low scattering structure for bow-tie patch and current carrier surface. Combined with the electromagnetic parameters such as dielectric constant and loss tangent of the 3-D printing medium substrate, the final antenna, as shown in Figure 3, simulation of radiation pattern is shown in Figure 4 by using HFSS software. The modeling simulation optimization is considered by using the neural network methods; and the most similar structural parameters were scanned.

Preprints (www.preprints.org) | NOT PEER-REVIEWED | Posted: 7 September 2022 doi:10.20944/preprints202209.0106.v1

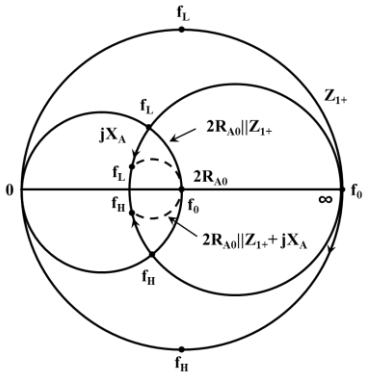

Figure 2. Tightly coupled dipole arrays usually achieve a bandwidth of more than 4 times the frequency.

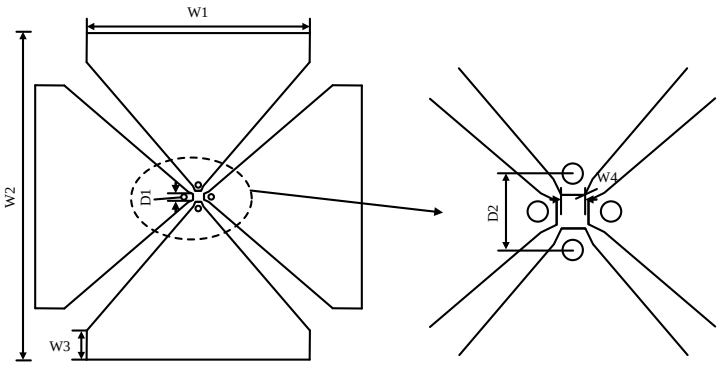

Figure 3. Two pairs of bow-tie shaped symmetric radiation object, geometry structure used in tightly coupled antenna array element.

Performance index of antenna element is shown as Table I, where the frequency from high to low are F3, FH, F0, FL, F2, F1, as listed in Table 1. The curve related to each frequency. After simulation, the performance of the antenna element can be archived the requirements. By the way, the Figure 4(a) shows the pattern of horizontal plane of the antenna element, and 4(b) pitch and elevation direction pattern of each frequency point of the antenna element. In order to improve the radiation efficiency and increase the bandwidth, the element size has been optimized, and we have obtained the final sizes of the designed antenna element structure, as listed in Table 2. In the following simulation procedure, all the sizes the table 2 will be used in the array element design.

Preprints (www.preprints.org) | NOT PEER-REVIEWED | Posted: 7 September 2022 doi:10.20944/preprints202209.0106.v1

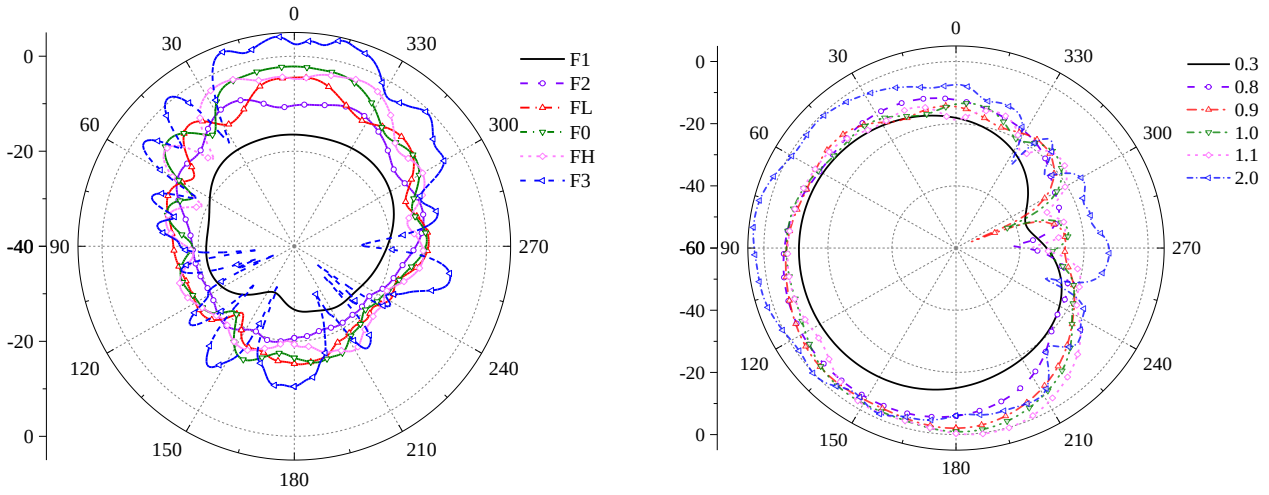

(**a**) (**b**)

Figure 4. Antenna element each frequency point pitch surface direction diagram, (**a**) Simulation results of the horizontal plane of the antenna element, (**b**) Pitch and elevation direction diagram of each frequency point of the antenna element.

Table 1. Antenna element performance indexes at six frequencies application.

	Frequency/GHz	Gain/dB	Horizontal beamwidth/°	Vertical beamwidth/°
F1	0.35	-19	90	60
F2	0.8	-13	120	90
FL	0.95	-1.5	70	70
F0	1.05	0	80	75
FH	1.15	0.5	80	80
F3	2.0	3	40	60

To meet the mounted platform, the design of a Bow-tie antenna array element uses the normal graphic design process, which can be met to metal powder coating print technology. Initially, a feeding network does not been considered. After dielectric substrate designed, it fabricated by the fused deposition modelling (FDM) technology processing in the 3-D printer. Then the antenna array is formed conformal to the substrate by using the microdroplet injection molding (MIM) technology. The detailed process will be discussed in the next section.

Preprints (www.preprints.org) | NOT PEER-REVIEWED | Posted: 7 September 2022 doi:10.20944/preprints202209.0106.v1

Table 2. Antenna element size in the structure of the Figure 3.

Demensions	W1	W2	W3	W4	D1	D2	D3	D4
Size(mm)	45	65	5.75	1.2	1.75	4	130.6	195

4. Manufacturing technologies based on FDM and MIM

4.1. Dielectric substrate material

The dielectric substrate is made of high temperature resistant SLA photosensitive resin, named JS-UV-LY02-G, which is a low-viscosity translucent. The machine parts manufactured by this material can bear 100~150°C temperature for a long time. It can withstand an instantaneous temperature of even 200°C. Therefore, the material has a good dimensional stability and detail reproduction, and can be used for making model hand plates and accessories that require temperature resistance, suitable for an industrial 3D printer with 355nm laser source. Some of the surface, optical and mechanical parameter properties of JS-UV-LY02-G are shown in Table 3 and Table 4, respectively. We use the material as our main antenna substrate design.

In Table 3, the laser source can be controlled according to requirement. For some materials, such as metal with higher melting point, we must choice the higher pulse probability to meet its printing.

Table 3. Surface and optical characteristics of JS-UV-LY02-G.

Surface properties		Optical properties		
Appearance	Translucent	Ec	11.3mJ/cm²	Critical exposure
Viscosity	340cps@30°C	Dp	0.115mm	Transmission depth: depth of cure vs. slope of Ln(E) curve
Density	1.14g/cm³	Build layer thickness	0.1mm	

Preprints (www.preprints.org) | NOT PEER-REVIEWED | Posted: 7 September 2022 doi:10.20944/preprints202209.0106.v1

Table 4. Mechanical properties of JS-UV-LY02-G Post UV curing.

Test Project	**Test Method**	**Value**	**Test Method**	**Value**
Tensile strength	ASTMD 638	65MPa	GB/T1040.1-2006	71MPa
Elongation at break	ASTMD 638	3~5%	GB/T1040.1-2006	3~5%
Bend strength	ASTMD 790	110MPa	GB/T9341-2008	115MPa
Bending modulus	ASTMD 790	2720MPa	GB/T9341-2008	2850MPa
Cantilever beam notched impact strength	ASTMD 256	20J/m	GB/T1843-2008	25J/m
Shore hardness	ASTMD 2240	87D	GB/T2411-2008	87D
Glass transition temperature	DMA tanθ peak	135℃	/	/
Thermal expansion coefficient(25~50℃)	ASTME831-05	50μm/m℃	GB/T1036-89	50μm/m℃
Thermal expansion coefficient(20~100℃)	ASTME831-05	150μm/m℃	GB/T1036-89	160μm/m℃

4.2. FDM hardware system

The FDM hardware system is composed of mechanical system and control system. An five-axis 3-D printing equipment, named 3D printer with integrated structure and function(Stratasys Objet 260 Connex1), and developed by the Key Laboratory of Electronic Equipment Structure Design of the Ministry of Education of Xidian University to realize big-size-area high-precision flexible circuit printing, which can be applied to touch screens, flexible photovoltaic, flexible OLED display/lighting, frequency-selective surfaces, conformal antennas and RFID. The ink is compatible with printheads such as Epson DX5 and DX7, Fuji Starlight and Spectra series, Konica KM512i and KM1024i, and Ricoh Gen5, Gen5s and Gen6 printheads. The performance of the samples printed with different printheads and conductive inks was tested and the results are shown in Table 5.

Preprints (www.preprints.org) | NOT PEER-REVIEWED | Posted: 7 September 2022 doi:10.20944/preprints202209.0106.v1

The mechanical system is composed of motion, nozzle, forming chamber, material chamber and other elements, mostly modular design, each element is independent of each other. The control system consists of a control cabinet and a power cabinet, which is used to control the movement of the nozzle and the temperature of the forming chamber, etc. The structure of the substrate to be printed in our approach is shown in Figure 5(a). To reduce the weight of the substrate and to ensure its dielectric properties, the interlayer between the two parabolic surfaces of the substrate is designed as a hollow structure with interconnected microscopic rods. After the FDM printer, the printed substrate is shown in the figure 5(b).

Table 5. Printing performance of different printheads and conductive inks.

Test item	BroadCON-INK550	BroadCON-INK550_KM	BroadCON-INK550_RH
Nozzles	Epson full series	Konica 512i, 1024iseries	Ricoh GEN5,GEN6
Silver powder particle size/nm	30~50	30~50	30~50
Viscosity/cp	5~6	~12	~10
Silver content/wt%	25~30	35~40	35~40
Square Resistance/mΩ/mil²	*1~2 Affected by curing conditions	*1~2 Affected by curing conditions	*1~2 Affected by curing conditions
Adhesion	0 level (100% No dislodging)	0 level (100% No dislodging)	0 level (100% No dislodging)
Hardness/H	2	2	2

Preprints (www.preprints.org) | NOT PEER-REVIEWED | Posted: 7 September 2022 doi:10.20944/preprints202209.0106.v1

(**a**) (**b**)

Figure 5. 3-D printing device and dielectric material, (**a**) FDM printer and (**b**) printed substrate

4.3. MIM of the conductive patterns

In order to use the inkjet printing technology better for the fabrication of metal film antenna structures, the dimensional resolutions and metal conductivities are essential issues to know the constraints of this fabrication method. The Stratasys Objet 260 Connex1 3-D printer has been used to inkjet print the dielectric material. The dielectric material used by the printer is a photosensitive polymer named VeroBlackPlus. The material has a dielectric constant of 2.6 and a loss tangent of 0.023. The printer has a layer resolution of 16 μm. In order to determine the lateral x–y resolution of the 3-D printer, narrow strips and gaps are printed, as shown in Fig. 6. This information is important for the realization of structures, as dimension becomes critical especially at higher frequencies. It is evident that the printer can reliably print features with widths and gaps of around 300 μm. This resolution is sufficient for the fabrication of microwave components.

For the inkjet printing of metal, the Dimatix 2831 materials printer has been used. A commercial silver nanoparticle-based ink from Sigma Aldrich (product 719048) with an average particle size of 150 nm is printed to form metal tracks on the 3-D printed dielectric. As inkjet printing is highly dependent on the substrate type, it is necessary to characterize

Preprints (www.preprints.org) | NOT PEER-REVIEWED | Posted: 7 September 2022 doi:10.20944/preprints202209.0106.v1

the ink on a particular substrate in order to obtain an accurate measure of the printing performance. Before printing, it is necessary to treat the surface of the substrate with acetone in order to remove unwanted contaminants such as grease and oils. Metal lines and gaps are inkjet-printed with a 20-μm-drop spacing and a 1-pL-drop volume cartridge. As is made clear in the image, the minimum line width of around 23 μm and gaps as narrow as 15 μm are realizable using inkjet printing. The surface of the inkjet-printed traces is slightly rough, as made visible in Fig. 5(b), which is due to the roughness of the 3-D printed substrate. The measured root-mean-square roughness is 6.4 μm. The conductivity of metal traces is critical for the performance of RF components.

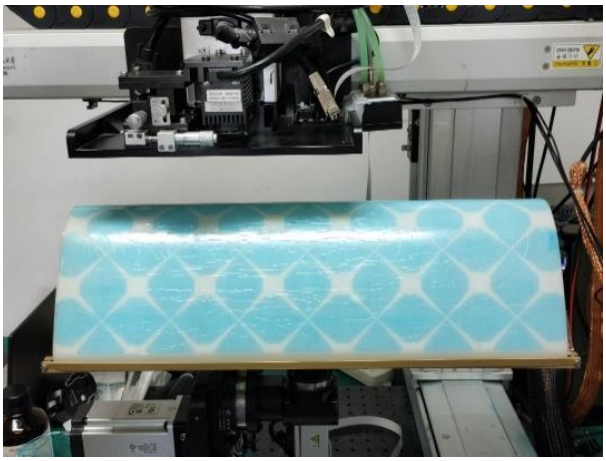

Figure 6. Designed antenna at fabricated platform.

The printed traces are subjected to heat so that the nanoparticles fuse together to form continuous metal tracks. This process is termed sintering. The conductivity of the metal traces increases with the duration of the sintering and temperature. Also, more layers can be printed to achieve higher conductivities. The resistance decreases by printing more layers and also by increasing the sintering duration. A minimum sheet resistance of around 1.3Ω

Preprints (www.preprints.org) | NOT PEER-REVIEWED | Posted: 7 September 2022 doi:10.20944/preprints202209.0106.v1

/sq. is achieved by printing 10 layers of silver ink giving a conductivity of around 3.8 × 105 S/m.

To ensure the stability of the conformal antenna forming performance and accuracy, the conductive pattern is printed on the media substrate before printing a layer of blue UV light-curing resin as a substrate material. Here the GH2220 nozzle special blue UV ink, which can be printed directly on various types of coated paper, white card, gray background white board, PVC card and other materials, fast drying speed, printing speed between 30 ~ 100 meters / hour. The product performance with much more stability, not clog the nozzle, drying speed, diffusion, chromaticity, etc. is very good. This ink has a strong waterproof function, especially suitable for printing without varnishing and without lamination products. The ink diameter of less than 1μm, does not contain volatile organic solvents, ultra-low viscosity, no irritating odor. Can ensure that the ink in the printing process without blocking the nozzle phenomenon. Long-term high-temperature storage test, no pigment coalescence, sinking, layering and other abnormal phenomena, and can be matched with various models of UV digital printing system on the market. After curing the ink layer of high hardness, good adhesion, scrub resistance, solvent resistance, high gloss, can also be customized without gloss, high level of sunlight resistance.

UV ink and weak solvent ink due to their own nature, determine their respective application methods and applications. In terms of structure, the biggest difference between UV inks and traditional solvent inks is, first of all, that they contain little or no volatile solvents (VOCs). Traditional solvent-based inks contain at least 50% volatile solvents, which is the essence of UV inks as environmentally friendly inks. Second, UV inks are generally

Preprints (www.preprints.org) | NOT PEER-REVIEWED | Posted: 7 September 2022 doi:10.20944/preprints202209.0106.v1

composed of 30-40% of the main resin, 20-30% of the active monomer, and a small amount of photoinitiators and similar leveling agents, defoamers and other additives. Among them, the main resin and the active monomer are reactive. The inkjet printout is also shown in the Figure 6.

5. Feed Structure Design

According to the system function requirements of the array, the structure-function integration design of the electrical transmission element and radiation element of the array is carried out, with the factors of electrical transmission, interface matching and line forming as the constraint requirements, and the common design optimization tools such as CAD/CAE/CAPP to realize the high integration of structure and function in the limited space range. The cable assembly is inserted into the antenna structure matrix through its side guide structure, and the solder pins are aligned with the antenna matrix opening, then four solder pins are welded and filled and fixed with potting material after the commissioning is qualified, as shown in Figure 7 and 8.

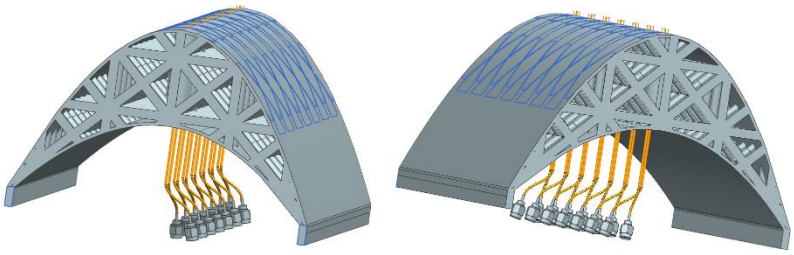

(**a**) (**b**)

Figure 7 Cable assembly inserted into the antenna array structure through its side guide structure, (**a**) main View, and (**b**) solder pins aligned with the antenna array opening, 7 ports symmetrically distributed in order.

Preprints (www.preprints.org) | NOT PEER-REVIEWED | Posted: 7 September 2022 doi:10.20944/preprints202209.0106.v1

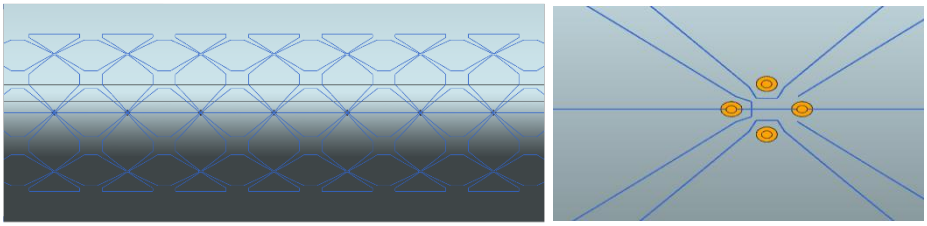

(**a**) (**b**)

Figure 8. Cable assembly inserted into the antenna array structure location, (**a**) top view on the conformal antenna side, (**b**) local view on one antenna element's fed point.

The antenna has been manufactured by a combination of 3-D inkjet printing of dielectric and 2D inkjet printing of metal. The helical structure along with the lens has been monolithically manufactured using a 3-D inkjet printer. This shows a major advantage of 3-D printing, as complex structures can be fabricated rapidly with the precise layer-by-layer deposition of material through a digitally controlled process. The print time for this 3-D geometry is 5 hours and 21 minutes with the available printer. An industrial-grade printer will take 40% less time to print the same geometry. The same metallization geometry has been used in the simulation, and it does not have a significant effect on the antenna performance. For mechanical support, two vertical posts have also been attached to the supporter after the metallization of the bow-tie array as shown in Fig. 6, which rest on the ground plane. The ground has been inkjet-printed separately because of the inkjet printer's limited work area, which cannot accommodate the complete structure. However, this will not be an issue if larger printers with more work volumes are used. After attaching the ground plane, the SMA connector is mounted on the antenna array for measurements.

6. Experiment and Design Method Verification

To verify our design, the radiation pattern of the proposed antenna array has been tested in our microwave anechoic chamber. Figure 9 shows the fabricated prototype and

Preprints (www.preprints.org) | NOT PEER-REVIEWED | Posted: 7 September 2022 doi:10.20944/preprints202209.0106.v1

testing scenario. Because the pattern was implemented in the H-plane, the array has little influence on the E-plane. Therefore, only the H-plane needs to be measured and analyzed. The simulation and measurement results of the radiation patterns in the H-plane are presented in Figure 10, where the simulation results are consistent with the measurement results in 0.3GHz, 0.8GHz, 0.9GHz, 1.0GHz, 1.1GHz and 2.0GHz. Therefore, the proposed antenna array can cover aviation and BeiDou navigation bands. Even in 300MHz, especially for rescue band, the measurement results of the radiation patterns are in very good agreement with simulation.

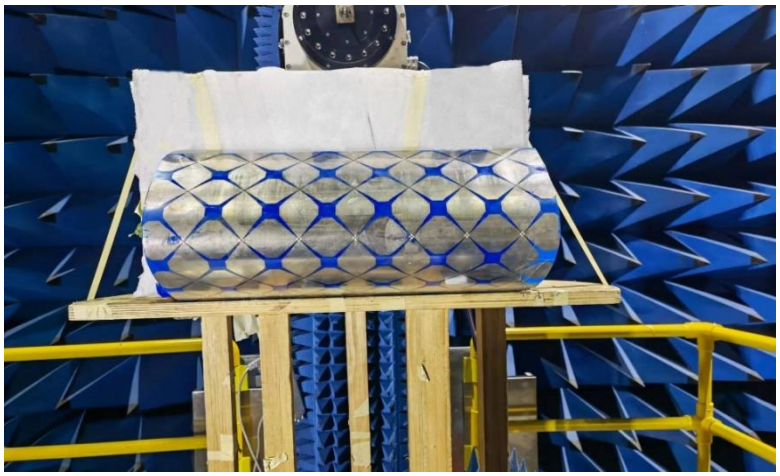

Figure 9. Test setup in the microwave anechoic chamber, z-axis point to the top of the antenna.

In Figure 10, we have obtained results in our laboratory. The microwave anechoic chamber is a spherical far-field testing system, with a far-field distance of 8m, frequency testing range of 300MHz ~ 18GHz, a static zone size of 1.8m, and a repetition error of ± 0.5dB.

The antenna array is designed with a total of 7 main ports. In order not to lose generality, edge units and intermediate units are selected as typical units for testing. Here, we choice 1, 3 and 4 unit, as shown in Figure 7, to record the testing results drown in the Figure 10.

Preprints (www.preprints.org) | NOT PEER-REVIEWED | Posted: 7 September 2022 doi:10.20944/preprints202209.0106.v1

In the figures, received electric field is used for the radiation pattern in the microwave anechoic chamber test, mainly shows the vertical polarization. The horizontal polarization unit has a long period, and its radiation characteristics are similar to those of the conventional tightly coupled antenna. The vertical polarization unit has a small period in the elevation plane. Therefore, the radiation characteristics of the vertical polarization unit are mainly verified.

Other units of the antenna have been tested in the same method. To save space, results are not shown here. In fact, the above results are sufficient to show that 3D printing technology has obvious advantages in realizing the design and manufacturing of conformal tightly coupled antennas.

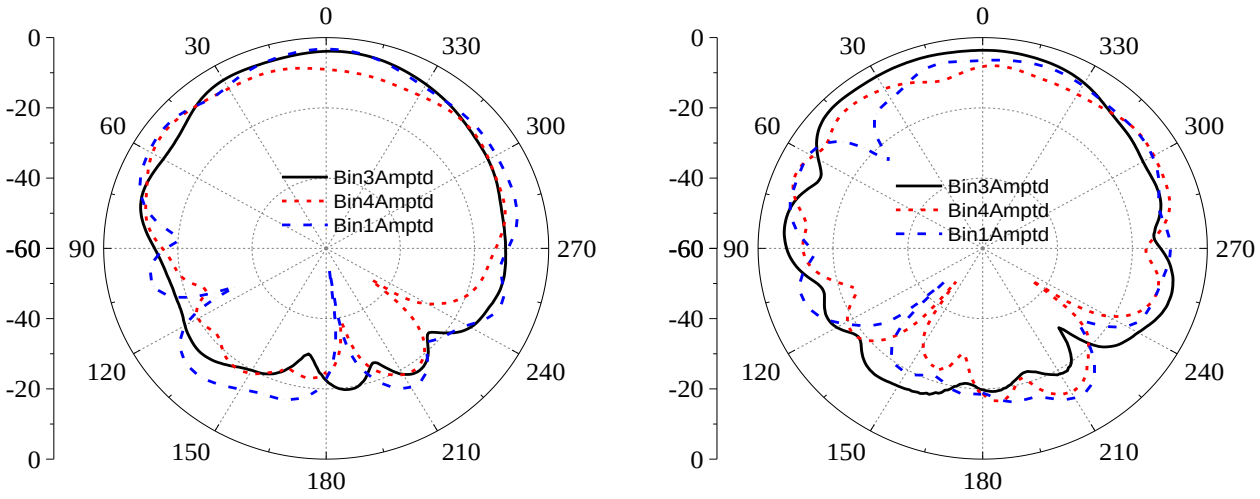

(**a**) (**b**)

Preprints (www.preprints.org) | NOT PEER-REVIEWED | Posted: 7 September 2022 doi:10.20944/preprints202209.0106.v1

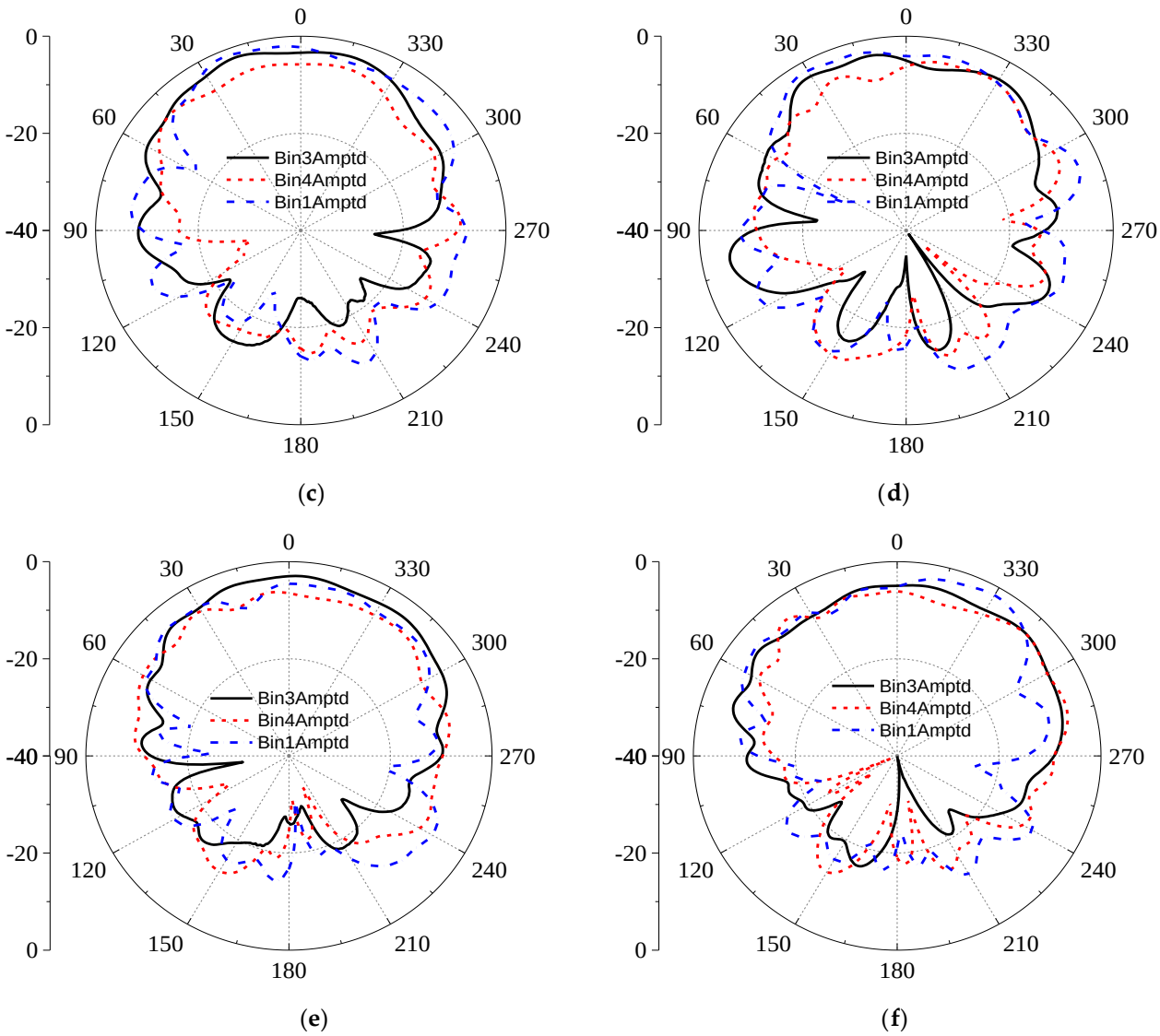

Figure 10. Experiment radiation pattern at horizontal plane in (**a**)0.3GHz; (**b**) 0.8GHz; (**c**) 0.9GHz; (**d**) 1.0GHz; (**e**) 1.1GHz; and (**f**) 2.0GHz.

7. Conclusion

This approach mainly focusses the application of 3-D printing technology in tightly coupled conformal antennas, which proves that conformal antennas based on the principle of tight coupling can be designed and printed with the current printing technology. With the increase of printing materials and layers, on the basis of this paper, we will continue to study the structural bearing characteristics of printing materials on conformal antennas and the impact of different materials on electrical performance parameters. By increasing the number

 doi:10.20944/preprints202209.0106.v1

of layers, it can expand the antenna bandwidth and optimize the electrical performance of the antenna, laying a foundation for the rapid processing of complex structure antennas in the future. Combining with 3-D printing technology, we simulated and designed a tightly coupled ultra-wideband conformal antenna, and completed the printing of substrate and radiators. Measurement results show in very good agreement with simulation. Through the conformal antenna processing, the 3-D printing technology gives us a very good application prospects. In this work, a bow-tie antenna array monolithically integrated with dielectric substrate. The integration has resulted in the airborne antenna fabricated conveniently. This work shows the utility of additive printing technologies to realize complex 3-D RF components that are very difficult and expensive to realize using conventional manufacturing techniques.

References

[1] J. Paulsen, M. Renn, K. Christenson, et al. Printing conformal electronics on 3D structures with aerosol jet technology// Future of Instrumentation International Workshop (FIIW), 2012. 2012:1-4.

[2] B. Munk, R. Taylor, T. Durharn, et al. A low-profile broadband phased array antenna, IEEE Antennas and Propagation Society International Symposium, 2003 AUG, vol. 2.

[3] M. –Y. Zhao, Y. –J. Zhu, T. Wang, et al. A wideband scanning circularly polarized array antenna based on the shorted transmission line model, IEEE ACCESS, vol. 10, 2022, pp. 78493-78501. DOI: 10.1109/ACCESS. 2022.3193692.

[4] M. Jones, J. Rawnick. A new approach to broadband array design using tightly coupled elements. IEEE Military Communications Conference, 2007, 1-7.

[5] S. Xiao, S. Yang, Y. Chen, et al. An ultra-wideband tightly coupled dipole array co-designed with low scattering characteristics, IEEE Transactions on Antennas and Propagation, 2019, vol. 67, no.1, pp.676-680.

[6] J. A. Kasemodel, C. -C. Chen, J. L. Volakis. Wideband planar array with integrated feed and matching network for wide-angle scanning. IEEE Transactions on Antennas and Propagation, 2013, vol. 61, no. 9, pp. 4528-4537.

[7] J. Wang, X. Zhao, Y. Ye and S. Liu. A millimeter-wave ultra-wideband tightly coupled dipole array antenna for vehicle communication, IEEE Antennas and Wireless Propagation Letters. 2022, Early access, DOI 10.1109/LAWP.2022.3193438.

[8] H. Zhang, S. Yang, S.-W Xiao, et al. Ultra-wide band phased antenna arrays based on tightly coupled open folded dipoles, IEEE Antennas and Wireless Propagation Letters, 2019, vol. 18, no. 2, pp.378-382.

[9] J. Wang, W. Cui, Y. Zhou, et al. Design of wideband antenna array with dielectric lens and defected ground structure, MDPI Electronics, vol.10, no.17, Aug. 2021.

[10] H. Xing, X. Wang, Z. Gao, et al. Efficient isolation of an MIMO antenna using defected ground structure, MDPI Electronics 2020, 9, 1265; doi:10.3390/electronics9081265.

[11] M. S. Kim, W. S. Chu, Y. M. Kim, et al. Direct metal printing of 3D electrical circuit using rapid prototyping. International Journal of Precision Engineering & Manufacturing, 2010, vol. 10, no. 5, pp.147-150.

[12] V. Gjokaj, J. Papapolymerou, J. D. Albrecht, et al. A compact receive module in 3-D printed Vivaldi antenna, IEEE Transactions on Components, Packaging and Manufacturing Technology, vol. 10, no. 2, FEB. 2020, pp. 343-346.

[13] I. Tzanidis, K. Sertel, J. L. Volakis. UWB low-profile tightly coupled dipole array with integrated balun and edge terminations, IEEE Transactions on Antennas and Propagation, 2013 vol. 61, no. 6, pp.3017-3025.

[14] L. Zhou, M. Tang, and J. Mao, 3-D printed Vivaldi antenna fed by SIW slot for millimeter-wave applications, 2021 IEEE International Conference on Microwave and Millimeter Wave Technology, pp:1-3, DOI: 10.1109/ ICMMT 52847. 2021.9617844.

[15] S. S. Holland, D. H. Schaubert, M. N. Vouvakis. A 7–21 GHz dual-polarized planar ultrawideband modular antenna (puma) array. IEEE Transactions on Antennas and Propagation, 2012, vol. 60, no. 10, pp. 4589-4600.

[16] J. Olivová, M. Popela, M. Richterová and Eduard Štefl. Use of 3D printing for horn antenna manufacturing. Electronics 2022, 11, 1539. https://doi.org/10.3390/electronics11101539.

[17] S. Agarwal, D. Masotti, S. Nikolaou and A. Costanzo. Conformal design of a high-performance antenna for energy-autonomous UWB Communication. Sensors 2021, 21, 5939. https://doi.org/ 10.3390/s21175939.

[18] Y. He, C. Oakley, P. Chahal, et al. Aerosol jet printed 24 GHz end-fire quasi-Yagi-Uda antenna on a 3-D printed cavity substrate, 2017 International Workshop on Antenna Technology: Small Antennas, Innovative Structures, and Applications (iWAT), 2017, pp.1-4.

[19] S. M. Sifat, M. M. Ali, S. I. Shams, et al. High gain bow-tie slot antenna array loaded with grooves based on printed ridge gap waveguide technology, IEEE ACCESS, vol. 7, 2019, pp.36177-36185, DOI:10.1109/ACCESS. 2019.2902596.

[20] J. T. Muth, D. M. Vogt, R. L. Truy, et al. Embedded 3D printing of strain sensors within highly stretchable elastomers. Advanced Meterials, 2014, vol. 26, no.36, pp.6307-12.

[21] M. F. Farooqui and A. Shamim, 3-D inkjet-printed helical antenna with integrated lens, IEEE Antennas and Wireless Propagation Letters, vol. 16, 2017, pp. 800-803.

Author Contributions: Conceptualization, L.H. and H.Z.; methodology, L.H.; validation, L.H., W.J. and P.Z.; formal analysis, W.T.; investigation, L.H.; resources, T.D.; data curation, L.Z.; writing—original draft preparation, L.H.; writing—review and editing, H.Z.; visualization, G.W.; supervision, G.W. and L.Z.; project administration, H.Z.; funding acquisition, T.D. and H.Z.; All authors have read and agreed to the published version of the manuscript. This work is supported by the National Natural Science Foundation of China and Key Research and Development Project of Hebei Province under Grants 62071166 and 21310401D, respectively.

Funding: This research is supported by the National Natural Science Foundation of China under Grant 62071166.

Conflicts of Interest: The authors declare no conflict of interest.